



BASIC SCIENCE ARTICLE

Novel variant in *BRAT1* with the lethal neonatal rigidity and multifocal seizure syndrome

Weixi Li¹, Shuiyan Wu¹, Huizhong Xu², Xiaoying Zhao³, Yizhi Pan¹, Hongbiao Huang¹, Haitao Lv¹, Xueping Zhu¹ and Ying Liu¹

BACKGROUND: Lethal neonatal rigidity and multifocal seizure syndrome (RMFSL) is caused by variants in *BRAT1* (BRCA1-associated protein required for ATM activation-1). However, the molecular mechanism of RMFSL is still unclear.

METHODS: An RMFSL infant was recruited and the peripheral blood samples from his trio-family were collected. The genomic DNA was extracted, and then the whole-exome sequencing was performed. The expression of *BRAT1* was analyzed by Western blotting. The subcellular localization of *BRAT1* and MitoSOX (mitochondrial superoxide level) was investigated by confocal microscopy. The RNA samples were obtained from transfected cells, and then the RNA sequencing was performed.

RESULTS: In this study, a novel homozygous *BRAT1* variant c.233G > C with amino acid change of R with P at residue 78 (R78P) was identified. This variant altered the peptide structure and subcellular localization, as well as the expression in vitro. However, R78P did not alter the ability of *BRAT1* to downregulate MitoSOX in mitochondria. Meanwhile, R78P *BRAT1* was positively correlated with temporal lobe epilepsy, autosomal recessive primary microcephaly, defective/absent horizontal voluntary eye movements, and neuron apoptotic process as indicated by gene set enrichment analysis (GSEA).

CONCLUSIONS: The *BRAT1* variant spectrum has been expanded, which will be helpful for genetic counseling. We also explored the molecular mechanism altered by R78P, which will provide a better understanding of the pathogenesis of RMFSL.

Pediatric Research (2022) 91:565–571; <https://doi.org/10.1038/s41390-021-01468-9>

IMPACT:

- The detailed course of an infant with lethal neonatal RMFSL was depicted.
- A novel disease-causing variant R78P in *BRAT1* for lethal neonatal RMFSL was identified.
- R78P led to reduced *BRAT1* expression and nuclear localization in vitro.
- R78P did not alter the ability of *BRAT1* to downregulate MitoSOX in the mitochondria.
- The variant R78P in *BRAT1* was positively correlated with temporal lobe epilepsy, autosomal recessive primary microcephaly, defective/absent horizontal voluntary eye movements, and neuron apoptotic process as indicated by GSEA.

INTRODUCTION

BRAT1 (BRCA1-associated protein required for ATM activation-1) is considered the disease-causing gene for lethal neonatal rigidity and multifocal seizure syndrome (RMFSL, MIM#614498), a condition that is usually clinically characterized by a small head, abnormal electroencephalogram (EEG), frequent multifocal seizures, hypoplasia of the frontal lobes, axial and limb rigidity, hypertonia and contractures, inability to swallow, intellectual disability, and sometimes visual problems.^{1–13} Initially, patients with *BRAT1* variants usually die from apnea or bradycardia before 4 months of age,¹ so this condition was called “lethal” for neonates. However, several individuals with *BRAT1* variants have been found to live for years,^{4,6,8,14–17} so “lethal” is not an appropriate description of the disease; some groups have renamed it as epilepsy of infancy with migrating focal seizures.¹⁸ Moreover, some *BRAT1* variant carriers do not necessarily have epilepsy^{8,17,19} and the symptom was diagnosed as nonprogressive

cerebellar ataxia.¹⁹ The reasons for the great clinical heterogeneity are as follows: (1) certain variants associated with *BRAT1*-related pathways that can modulate their phenotypes; (2) hypomorphic allele(s) that can ameliorate their phenotypes; and (3) variants in different domains that may modulate the severity.¹⁷ In summary, *BRAT1* variants can result in moderate to severe presentations, defined by later-onset epilepsy and survival past infancy.¹⁷

The disease-causing gene *BRAT1* is located at chromosome 7p22.3, and encodes a protein of 821 amino acids, with a CIDE (cell death-inducing DFF-45 like effector) domain (amino acids (a.a.) 54–95), and two HEAT (*Huntingtin*, *Elongation factor 3*, *A* subunit of protein phosphatase 2A, and *TOR1*) repeat domains (a.a. 495–531, 544–576).²⁰ *BRAT1* regulates the stability of ataxia telangiectasia (ATM) and DNA-dependent protein kinase (DNA-PK) with its C terminus (a.a. 176–821), which indicates the involvement of cell growth.^{21,22} *BRAT1* is also essential for the phosphorylation of ATM and DNA-PK, and mediates the DNA

¹Institute of Pediatric Research, Children’s Hospital of Soochow University, Suzhou, Jiangsu Province, People’s Republic of China; ²Institute for Advanced Study and School of Physical Science and Technology, Soochow University, Suzhou, Jiangsu Province, People’s Republic of China and ³First Affiliated Hospital of Anhui Medical University, Hefei, Anhui Province, People’s Republic of China

Correspondence: Ying Liu (d201077400@alumni.hust.edu.cn)

These authors contributed equally: Weixi Li, Shuiyan Wu, Huizhong Xu.

Received: 12 November 2020 Accepted: 27 February 2021

Published online: 31 March 2021

damage response.²⁰ *BRAT1* can also form a complex with BRP1 and prevent transcriptional silencing.²³ *BRAT1* deficiency induces apoptosis of mouse embryonic fibroblasts and the human osteosarcoma U2OS cell line,^{21,22} as well as increased glucose metabolism and mitochondrial malfunction.² However, the disorder caused by *BRAT1* variants is unlikely to result from defective ATM kinase or dysfunctional mitochondria.¹⁹ The pathogenesis of the syndrome needs to be explored.

In this study, a novel homozygous *BRAT1* variant c.233G > C with an amino acid change of R with P at residue 78 (R78P) was identified in a Chinese infant with RMFSL. This variant might alter the peptide structure because the mutated residue formed two fewer hydrogen bonds. The expression of R78P *BRAT1* was significantly decreased in cells as indicated by Western blotting. In addition, there was significantly less localization of R78P *BRAT1* in the nucleus, which was proven by both confocal microscopy and Western blotting. Gene set enrichment analysis (GSEA) results proved that R78P *BRAT1* was positively correlated with temporal lobe epilepsy, autosomal recessive primary microcephaly, and defective/absent horizontal voluntary eye movements, which were among the main symptoms of RMFSL.

METHODS

Subject

The male patient with RMFSL in a trio-family was recruited at the Children's Hospital of Soochow University. The proband underwent a careful physical examination. This study followed the Declaration of Helsinki and was approved by the ethics committee of the Children's Hospital of Soochow University ethics committee (No. 2020CS059). Written consent was obtained from the parent before they participated in the whole-exome sequencing.

Exome sequencing and variant detection

Genomic DNA was extracted from peripheral blood of the trio-family by a Blood & Cell Culture DNA Mini kit (Qiagen) and was examined by a Nanodrop 2000 (Thermo). Exome sequencing libraries were constructed using the SureSelectXT Human All Exome V6/V6 + UTRs kit (Agilent). The PCR products were validated via an Agilent 2100 Bioanalyzer (Agilent). The exons were captured by Dynabeads MyOne Streptavidin T1 magnetic beads. The libraries were loaded onto the Illumina NextSeq 500 for sequencing. The primary analysis was performed via built-in software, HiSeq Control Software (HCS), and RTA 2.3 plus, and demultiplexing was performed via bcl2fastq 2.17. Finally, the raw data from exome sequencing were analyzed using bioinformatics programs. The reads were mapped to the human reference genome (hg19). The single-nucleotide polymorphisms and INDELs were analyzed by HaplotypeCaller and annotated by ANNOVAR. The pathogenicity of variants was analyzed according to the ACMG (American College of Medical Genetics and Genomics) standards and guidelines. The target exome regions had a mean depth of coverage of 155.03 times. A total of 98.84% of the exomes were covered at least ten times.

Cell culture

The 293T cells (ATCC® CRL-3216™) were purchased from ATCC (Manassas, VA, USA). Cells were incubated in Dulbecco's modified Eagle's medium with 10% fetal bovine serum and 1% penicillin–streptomycin solution at 37 °C with 5% CO₂.

Plasmid construction

The wild-type (WT) and mutated *BRAT1* complementary DNA (cDNA) were synthesized and cloned into pEGFP-N1 vectors, respectively. The *BRAT1* sequence in plasmids was confirmed by Sanger sequencing.

Transient transfection

The 293T cells were seeded in plates at a density of 3.5×10^5 cells/ml. After 24 h, plasmids were transfected into cells using Lipofectamine 3000 (Invitrogen) according to the manufacturer's instructions.

The expression analysis

Forty-eight hours after transfection of 1.5 µg plasmids in a 12-well plate, 293T cells were washed with phosphate-buffered saline (PBS) buffer and treated with RIPA lysis buffer. The products were collected and analyzed by Western blotting. GFP tag mouse monoclonal antibody (66002-1-Ig, Proteintech) and the antibody against glyceraldehyde 3-phosphate dehydrogenase (GAPDH) (10494-1-AP, Proteintech) were used. The bands were calculated by Gel-Pro analyzer 4 (Media Cybernetics, L.P.).

Subcellular localization of *BRAT1*

The GFP-tagged *BRAT1* WT and R78P plasmids were transfected into 293T cells, respectively. After 48 h, the cells were washed with PBS and incubated with Hoechst 33342 for 5 min. Then, the Hoechst 33342 was removed and cells were washed with PBS for three times and imaged by confocal microscopy (Olympus) immediately.

Nuclear Protein Extraction kit

Forty-eight hours after transfection of 1.5 µg plasmids in a 12-well plate, 293T cells were washed with PBS buffer and then treated with Nuclear Protein Extraction kit (R0050, Solarbio), according to the manufacturer's instructions. The products were collected and analyzed by Western blotting. GFP tag mouse monoclonal antibody (66002-1-Ig, Proteintech), antibody against GAPDH (10494-1-AP, Proteintech), and antibody against Lamin A/C (ab108595, Abcam) were used. The bands were calculated by Gel-Pro analyzer 4 (Media Cybernetics, L.P.).

Mitochondrial superoxide level

Forty-eight hours after transfection with GFP-tagged *BRAT1* WT or R78P plasmids in chambers, 293T cells were treated with MitoSOX™ Red Mitochondrial Superoxide Indicator (M36008, Thermo) according to the manufacturer's protocol, followed by nuclear staining with Hoechst 33342. Mitochondrial superoxide level (MitoSOX) was analyzed by confocal microscopy (Olympus). The mean intensity of MitoSOX red was calculated by ImageJ 1.52p (National Institutes of Health, USA).

RNA extraction, cDNA library preparation, and RNA sequencing (RNA-seq)

A total of 3×10^6 293T cells were transfected with 4 µg *BRAT1* WT or R78P plasmids in a 6-well plate. After 48 h, total RNA was extracted from the samples using TRIZOL (Life science) and the DNA-free kit (Ambion). Three micrograms of RNA per sample was used as input material for RNA sample preparations. The sequencing libraries were generated with NEBNext Ultra™ RNA Library Prep kit for Illumina (NEB, USA) following the manufacturer's protocol. The integrity and quality of cDNA libraries were analyzed with Agilent 2100 Bioanalyzer and ABI StepOne plus Real-Time PCR System. The mapping of 100-bp paired-end reads to genes was undertaken using HTSeq v0.6.0 software.

RESULTS

Clinical presentation

The male proband was born to nonconsanguineous normal parents as the first child after a 39-week pregnancy, the birth weight was 3650 g (+1.1 SD), the birth length was 49 cm (−0.9 SD), and the head circumference (HC) was 33.5 cm (−0.4 SD). He was fed with breast milk and was vaccinated on time. When he was at the age of 1 month and 2 days, he was found to have frequent eye blinking, fisted hands, rigidity, and shaking limbs,

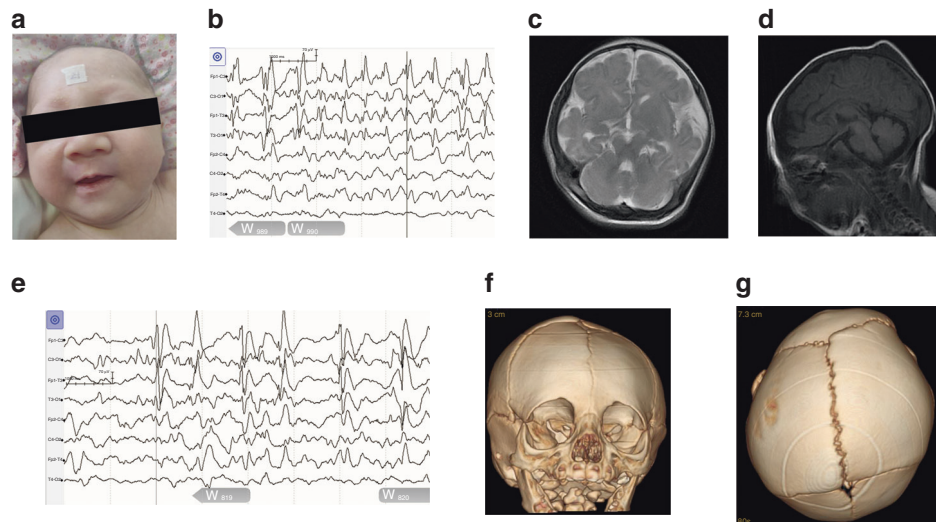


Fig. 1 Clinical presentation of the proband. **a** The dysmorphic facial features, such as sparse eyebrows, micrognathia, and a small head. **b** The initial electroencephalogram (EEG) showed more sharp wave discharges in the left forehead-parietal region than in the right forehead-parietal region. **c** Bilateral frontal and temporal subarachnoid space was widened. **d** Corpus callosum was thin. **e** A second EEG showed focal sharp wave discharges and spike and slow-wave complexes in the left forehead-temporal region when the proband was 2 months old. **f** Small and anisopleural frontal bones. **g** Overlapping cranial sutures.

without any apparent causes. The paroxysmal convulsions usually lasted for ~10 s and then stopped spontaneously. This happened ~30 times per day. When he was referred to us 2 days later, his dysmorphic features, which were sparse eyebrows, micrognathia, and a small head, were noticed (Fig. 1a), and his HC was 34 cm (<-2SD). Moreover, he presented hoarse crying, decreased activity, muscular hypertonia, hyperactive deep tendon reflexes, and positive Babinski's sign. He neither stared at the light source nor turned his head to follow a horizontally moving object. However, no optic problems were found by fundus examination (Fig. S1). The initial EEG showed more sharp wave discharges in the left forehead-parietal region than in the right forehead-parietal region (Fig. 1b). Brain magnetic resonance imaging indicated that the bilateral frontal and temporal subarachnoid space was widened (Fig. 1c), and the corpus callosum was thin (Fig. 1d). Laboratory examination, which included routine blood examination, blood gas analysis, measurement of microelements, blood glucose, and serum ammonia, the TORCH panel, and cerebrospinal fluid and metabolic screening, did not reveal any abnormalities.

During hospitalization, he was treated with phenobarbital (which was stopped due to allergy), levetiracetam, or levetiracetam combined with topiramate for ~1 month. However, the treatment was not effective in controlling the seizures, as indicated by a second EEG examination performed when he was 2 months of age. The EEG showed focal sharp wave discharges and spike and slow-wave complexes in the left forehead-temporal region (Fig. 1e). Volume rendering and multiplanar reconstruction results showed small and asymmetrical frontal bones (Fig. 1f) and overlapping cranial sutures (Fig. 1g) when he was 2.5 months old. At that time, his weight was still normal (3670 g, -1.6 SD), whereas his HC was still small (36.5 cm, <-2SD). However, his neurological symptoms progressed into intractable myoclonic seizures that were associated with recurrent respiratory tract infections and dysphagia at the age of 6 months. He died of respiratory infection and malnutrition, weighing 5500 g (<-2SD), at the age of 7 months.

A novel missense variant in *BRAT1* was identified. Peripheral blood samples from the proband (II: 1) and his normal parents (I: 1, I: 2) were collected (Fig. 2a), and genomic DNA was

isolated for whole-exome sequencing. A homozygous missense variant c.233G > C in *BRAT1* (NM_152743) was identified in the proband (Fig. 2b), while his normal parents (I: 1 and I: 2) were both heterozygous carriers (Fig. S2). The variant led to the replacement of R78P of the coding protein, which is located in the CIDE domain (Fig. 2c). The amino acid in this residue was evolutionarily conserved (Fig. 2d), which indicated an important functional role. R78P was predicted to be disease-causing in MutationTaster (<http://www.mutationtaster.org/>). The 3D structures of WT and mutated proteins were constructed in SWISS-MODEL (<https://swissmodel.expasy.org/>), and the hydrogen bonds were analyzed by PyMOL (Fig. 2e). The mutated P78 was only predicted to form hydrogen bonds with T82, while the WT R78 was predicted to form two additional hydrogen bonds with S74 and F75. The hydrogen bond alterations caused by R78P might lead to misfolding and affect its function. However, as the bioinformatic analysis was not strong enough to elucidate pathogenesis, more functional work was performed as follows.

R78P *BRAT1* was downregulated and its localization was altered. As the variant was predicted to be disease-causing, alterations in function caused by the variant were investigated. Identical doses of GFP-tagged WT and R78P *BRAT1* plasmids were transfected into 293T cells, and protein expression was examined by Western blotting (Fig. 3a). The results indicated that R78P *BRAT1* was significantly downregulated in vitro (Fig. 3b).

Subcellular localization was also investigated by confocal microscopy. When the GFP-tagged WT and R78P *BRAT1* plasmids were transfected into 293T cells, the localization of *BRAT1* differed greatly. WT *BRAT1* was diffusely expressed in both the cytoplasm and the nucleus, while R78P *BRAT1* was expressed mainly in the cytoplasm and only scarcely in the nucleus (Fig. 3c). The mean intensity of the GFP signal in the nucleus and cytoplasm was analyzed by ImageJ, and the ratio of the mean GFP intensity in the nucleus to that in the cytoplasm was calculated by GraphPad Prism. The ratio of R78P *BRAT1* localization in the nucleus to that in the cytoplasm was significantly decreased (Fig. 3d).

To clarify whether *BRAT1* could translocate into the nucleus, a Nuclear Protein Extraction kit was used, and the expression in the nucleus and cytoplasm was examined by Western blotting (Fig. 3e).

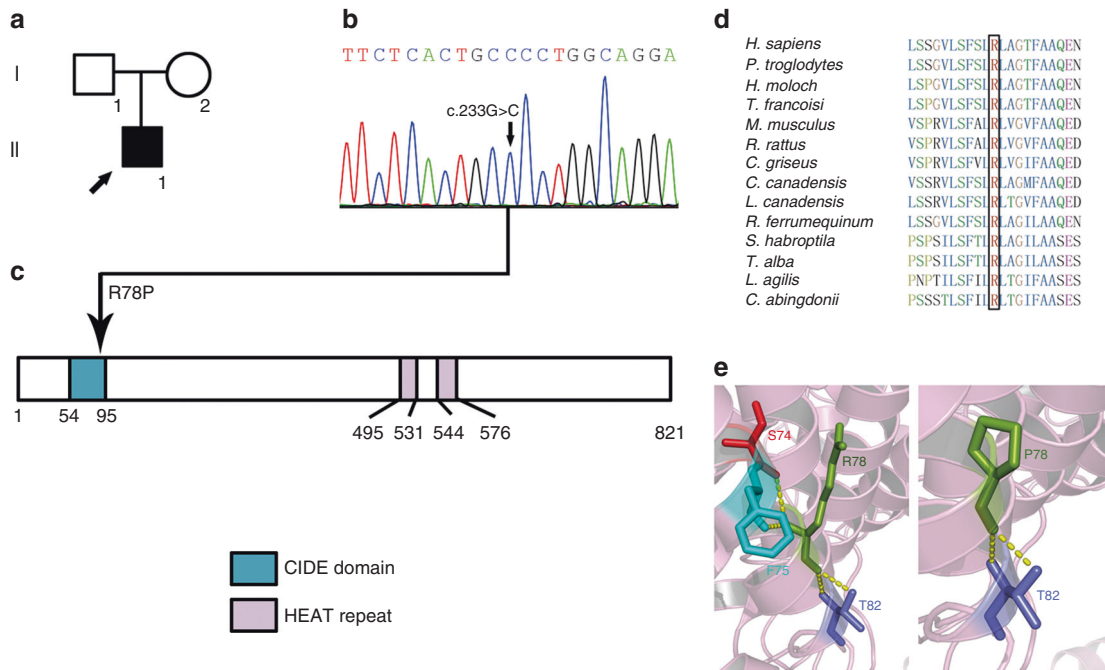


Fig. 2 The genetic analysis. **a** The information of the pedigree. The proband was indicated by an arrow. **b** Sanger sequencing result of the variant. **c** Protein structure of BRAT1. **d** The residue R78 indicated in the box was evolutionarily conserved. **e** The mutated P78 was predicted to form hydrogen bonds with T82 (right), while the wild-type R78 was predicted to form two additional hydrogen bonds with S74 and F75 (left).

The results indicated that WT and R78P BRAT1 could both be expressed in the nucleus and cytoplasm, while the expression of R78P BRAT1 in the nucleus was significantly lower than that of WT BRAT1 (Fig. 3f).

Both WT and R78P BRAT1 could downregulate MitoSOX
As BRAT1 deficiency leads to increased MitoSOX², we wondered whether R78P BRAT1, which is less abundantly expressed in cells, could regulate MitoSOX. Therefore, we examined MitoSOX in 293T cells transfected with GFP-tagged WT or R78P BRAT1 plasmids (Fig. 3g). The MitoSOX in BRAT1-overexpressing cells was significantly decreased compared to that in NC cells. However, R78P BRAT1 also preserved the ability to downregulate MitoSOX (Fig. 3h). The results indicated that R78P did not alter the ability of BRAT1 to downregulate MitoSOX.

The alteration of transcription caused by R78P
To explore which pathways could be affected by R78P, RNA-seq was performed. We aimed to identify the pathways associated with the phenotypes of RMFSL. RNA samples were collected from 293T cells that had been transfected with WT and R78P BRAT1 plasmids and then cultured for an additional 48 h. The RNA-seq results showed that 2553 genes were downregulated and 2350 genes were upregulated by R78P (Fig. 4a). With GSEA, we noticed that R78P BRAT1 was positively correlated with temporal lobe epilepsy (Fig. 4b), autosomal recessive primary microcephaly (Fig. 4c), defective/absent horizontal voluntary eye movements (Fig. 4d), and neuron apoptotic process (Fig. 4e). The neuron apoptotic process identified by GSEA was in accordance with “apoptosis” identified in KEGG (Kyoto Encyclopedia of Genes and Genomes) enrichment analysis (Fig. 4f).

DISCUSSION

In this study, we recruited an infant with RMFSL and identified the novel homozygous missense variant c.233G>C in *BRAT1*, which led to R78P in the coded protein. The variant led to reduced

BRAT1 expression and nuclear localization in vitro. However, R78P did not disturb the ability of BRAT1 to downregulate MitoSOX. R78P BRAT1 significantly altered the transcription of 4903 genes and was positively correlated with temporal lobe epilepsy, autosomal recessive primary microcephaly, and defective/absent horizontal voluntary eye movements, which are among the main symptoms of RMFSL. The pathogenesis of RMFSL caused by R78P BRAT1 may be associated with apoptosis as indicated by GSEA and KEGG enrichment analysis.

In fact, the CIDE domain of BRAT1, in which the variant causing R78P is located, is associated with DNA fragmentation,²⁴ which is a hallmark of apoptosis. CIDE is a conserved N-terminal region that possesses two α -helices and five β -strands, as determined by nuclear magnetic resonance spectroscopy.²⁵ Therefore, the alteration of hydrogen bonds caused by R78P might lead to domain misfolding and affect its function in the apoptosis pathway. However, we could not perform autopsy or assess the apoptosis situation in the brain tissue of the proband. Perhaps, BRAT1 knock-in or knock-out animal models are needed to determine the association between apoptosis and RMFSL.

Other molecular mechanisms of the disorder caused by variants in BRAT1 have also been explored. In a previous report that focused on V62E BRAT1, the expression of the mutant protein in patient-derived cell lines was significantly decreased,¹⁹ which was in accordance with our result of reduced expression of R78P BRAT1 in vitro. The group also claimed that there were no significant differences in PDH E1 α S293 expression or oxygen consumption rates between the patient calls and the parental control cells, which indicated that the disorder is unlikely to result from mitochondrial dysfunction.¹⁹ This opinion was supported by our results, in which we found that R78P BRAT1 could downregulate MitoSOX in the mitochondria, similar to WT BRAT. Thus, more functional work is needed to elucidate how variants in BRAT1 lead to this disorder.

In a previous report, mutated BRAT1 (c.638_639insA) did not localize to the nucleus.¹ However, in our results, BRAT1 R78P could

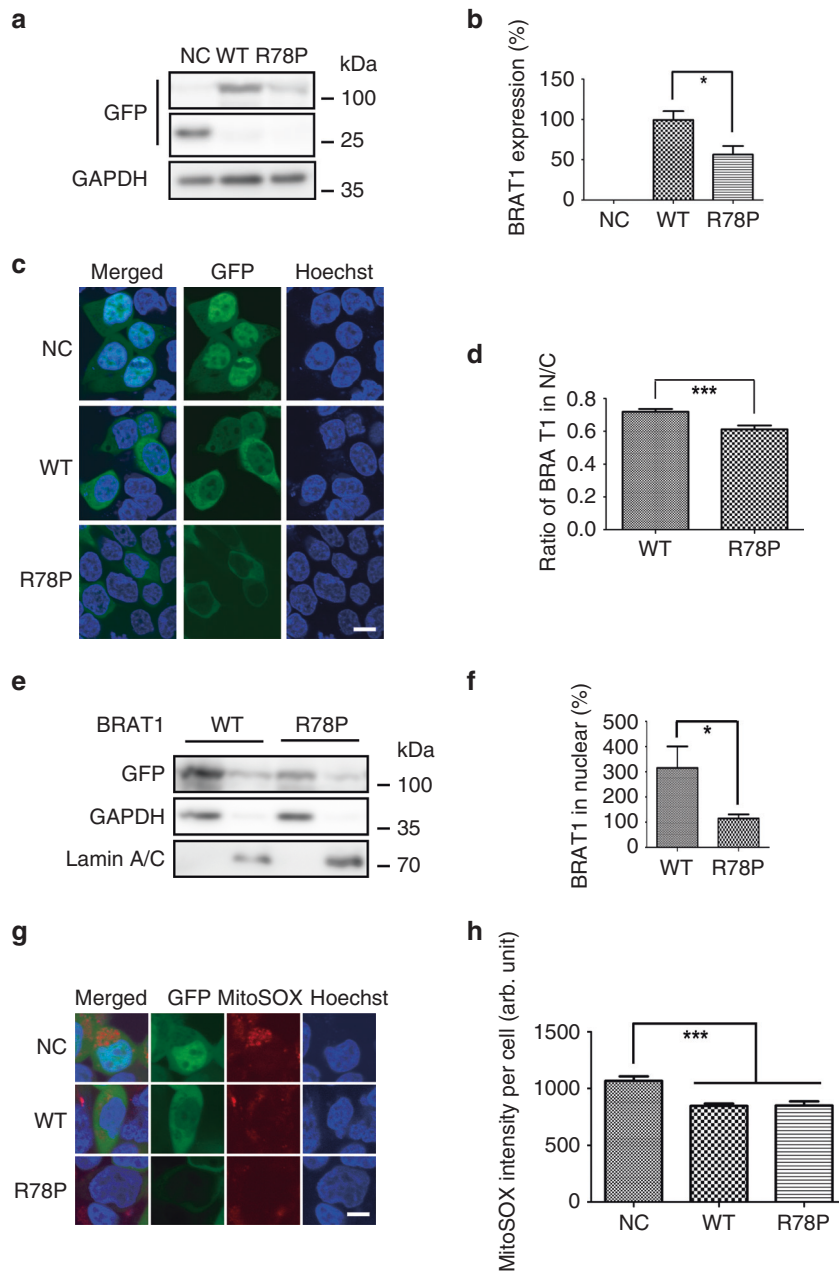


Fig. 3 The expression and subcellular localization of wild-type and R78P BRAT1. **a** R78P BRAT1 was significantly downregulated compared to WT in vitro, as indicated by Western blotting. **b** The intensity of the bands was quantified by Gel-Pro analyzer. **c** WT BRAT1 was diffusely expressed in both the cytoplasm and the nucleus, while R78P BRAT1 was expressed mainly in the cytoplasm and only scarcely in the nucleus. **d** The mean intensity of GFP in the nucleus and cytosol was quantified by ImageJ, and the ratio was calculated. **e** WT and R78P BRAT1 could both be expressed in the nucleus and cytoplasm, while the expression of R78P BRAT1 in the nucleus was significantly lower than that of WT BRAT1. **f** The intensity of the bands was quantified by Gel-Pro analyzer. **g** R78P BRAT1 preserved the ability to downregulate MitoSOX as WT did. **h** Mean intensity of MitoSOX in each cell, which was transfected with GFP-tagged plasmids. The mean intensity of MitoSOX was calculated in at least ten cells by ImageJ. There was no significant difference between WT and R78P. The scale bar indicated 10 μ m. All data were calculated by GraphPad Prism 5 and analyzed by *t* test. **P* < 0.05 and ****P* < 0.001.

still localize to the nucleus, although it was significantly less abundant than WT BRAT1. We suspect that c.638_639insA was a frameshift variant that disrupted the secondary and tertiary structures of the protein much more severely than the missense variant c.233G > C in this report. For example, there were three nuclear localization sequences (NLSs) in BRAT1, as predicted by NLS Mapper (http://nls-mapper.iab.keio.ac.jp/cgi-bin/NLS_Mapper_y.cgi): "357-SKSSCAGLLCRTLALHLEELQLPQRPSPW," "476-RWLLSPPKTPGCS DLGPLIPQFLRELPVLQKRL," and "499-RELPVLQKRLCHPCWEVRDSA-LEFLTQLSRHWG(G)." All three were behind the frameshift variant

residue, so the NLSs were all changed. On the other hand, since R78P is in front of the NLSs, BRAT1 R78P retained some of its ability to be transported into the nucleus.

In summary, we identify a novel and likely pathogenic missense variant in BRAT1. The BRAT1 variant spectrum has been expanded, which will be helpful for genetic counseling. We also explored the molecular mechanism altered by R78P, which will provide a better understanding of the pathogenesis of RMFSL. However, more functional work in vivo is needed to clarify the molecular mechanism of RMFSL in the future.

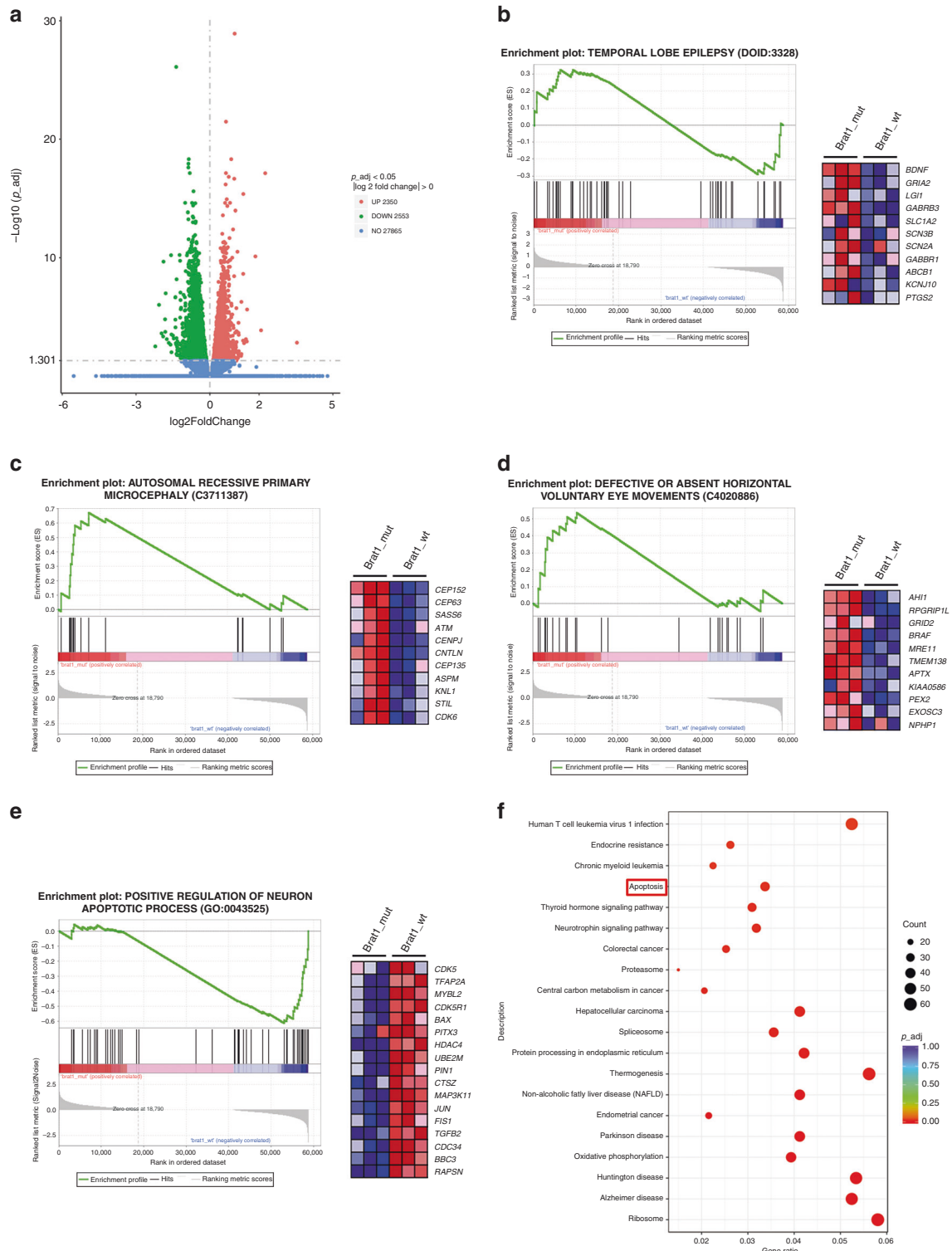


Fig. 4 The RNA-seq results. **a** The volcano plot of the genes altered by R78P in *BRAT1*. Two thousand three hundred and fifty genes were upregulated, whereas 2553 genes were downregulated. **b** R78P *BRAT1* was positively correlated with temporal lobe epilepsy, **c** autosomal recessive primary microcephaly, **d** defective/absent horizontal voluntary eye movements, and **e** neuron apoptotic process as indicated by GSEA. All the associated genes were listed. *Brat1_mut* indicated R78P *BRAT1* and *brat1_wt* indicated WT *BRAT1*. **f** The apoptosis pathway was also supported by KEGG enrichment analysis.

ACKNOWLEDGEMENTS

We would like to thank the family for joining in the study. We thank Jin Ma for the technical support. This work was supported by the National Natural Science Foundation of China (Nos. 81803116, 81570455, 81870365, and 81570125) for

work designing and whole-exome sequencing, the Basic Research Project for Medical and Health Applications of Suzhou City (Nos. SYS2018077, SYS2019083, and SYS201757) for reagent purchasing, the Jiangsu Province's Science Technology Support Program (Social Development) Project (BE2017658) and

Startup fund (Q410800320) from Soochow University for data collection, and Jiangsu Province Medical Key Talents (ZDRCA2016049) for analyzing data and writing the report.

AUTHOR CONTRIBUTIONS

W.L. and X. Zhao were responsible for the diagnosis and treatment of the patient. Y.P. analyzed the EEG results. H.H. analyzed the RNA-seq results. H.L., X. Zhu, H.X., and Y.L. designed the project. W.L., S.W., and H.X. performed the experiments. Y.L. wrote the manuscript and H.X. revised it.

ADDITIONAL INFORMATION

Supplementary information The online version contains supplementary material available at <https://doi.org/10.1038/s41390-021-01468-9>.

Competing interests: The authors declare no competing interests.

Statement of consent Written consent was obtained from the proband's parent.

Publisher's note Springer Nature remains neutral with regard to jurisdictional claims in published maps and institutional affiliations.

REFERENCES

1. Puffenberger, E. G. et al. Genetic mapping and exome sequencing identify variants associated with five novel diseases. *PLoS ONE* **7**, e28936 (2012).
2. So, E. Y. & Ouchi, T. *BRAT1* deficiency causes increased glucose metabolism and mitochondrial malfunction. *BMC Cancer* **14**, 548 (2014).
3. van de Pol, L. A. et al. Early-onset severe encephalopathy with epilepsy: the *BRAT1* gene should be added to the list of causes. *Neuropediatrics* **46**, 392–400 (2015).
4. Saitsu, H. et al. Compound heterozygous *BRAT1* mutations cause familial Ohtahara syndrome with hypertonia and microcephaly. *J. Hum. Genet.* **59**, 687–690 (2014).
5. Straussberg, R. et al. Lethal neonatal rigidity and multifocal seizure syndrome—report of another family with a *BRAT1* mutation. *Eur. J. Paediatr. Neurol.* **19**, 240–242 (2015).
6. Hanes, I., Kozenko, M. & Callen, D. J. A. Lethal neonatal rigidity and multifocal seizure syndrome—a misnamed disorder? *Pediatr. Neurol.* **53**, 535–540 (2015).
7. Srivastava, S. & Naidu, S. Epileptic encephalopathy due to *BRAT1* pathogenic variants. *Pediatr. Neurol. Briefs* **30**, 45 (2016).
8. Fernández-Jaén, A. et al. Mutations in *BRAT1* cause autosomal recessive progressive encephalopathy: report of a Spanish patient. *Eur. J. Paediatr. Neurol.* **20**, 421–425 (2016).

9. Celik, Y., Okuyaz, C., Arslankoylu, A. E. & Ceylaner, S. Lethal neonatal rigidity and multifocal seizure syndrome with a new mutation in *BRAT1*. *Epilepsy Behav. Case Rep.* **8**, 31–32 (2017).
10. Van Ommeren, R. H., Gao, A. F., Blaser, S. I., Chitayat, D. A. & Hazrati, L. *BRAT1* mutation: the first reported case of Chinese origin and review of the literature. *J. Neuropathol. Exp. Neurol.* **77**, 1071–1078 (2018).
11. Szymanska, K. et al. Clinico-pathological correlation in case of *BRAT1* mutation. *Folia Neuropathol.* **56**, 362–371 (2018).
12. Valence, S. et al. Exome sequencing in congenital ataxia identifies two new candidate genes and highlights a pathophysiological link between some congenital ataxias and early infantile epileptic encephalopathies. *Genet. Med.* **21**, 553–563 (2019).
13. Oatts, J. T., Duncan, J. L., Hoyt, C. S., Slavotinek, A. M. & Moore, A. T. Inner retinal dystrophy in a patient with biallelic sequence variants in *BRAT1*. *Ophthalmic Genet.* **38**, 559–561 (2017).
14. Horn, D. et al. *BRAT1* mutations are associated with infantile epileptic encephalopathy, mitochondrial dysfunction, and survival into childhood. *Am. J. Med. Genet. A* **170**, 2274–2281 (2016).
15. Smith, N. J., Lipsett, J., Dibbens, L. M. & Heron, S. E. *BRAT1*-associated neurodegeneration: intra-familial phenotypic differences in siblings. *Am. J. Med. Genet. A* **170**, 3033–3038 (2016).
16. Mundy, S. A., Krock, B. L., Mao, R. & Shen, J. J. *BRAT1*-related disease—identification of a patient without early lethality. *Am. J. Med. Genet. A* **170**, 699–702 (2016).
17. Srivastava, S. et al. *BRAT1* mutations present with a spectrum of clinical severity. *Am. J. Med. Genet. A* **170**, 2265–2273 (2016).
18. Scheffer, I. E. et al. *BRAT1* encephalopathy: a recessive cause of epilepsy of infancy with migrating focal seizures. *Dev. Med. Child Neurol.* **62**, 1096–1099 (2019).
19. Mahjoub, A. et al. Homozygous pathogenic variant in *BRAT1* associated with nonprogressive cerebellar ataxia. *Neurol. Genet.* **5**, e359 (2019).
20. Ouchi, M. & Ouchi, T. Regulation of ATM/DNA-PKcs phosphorylation by *BRCA1*-associated *BAAT1*. *Genes Cancer* **1**, 1211–1214 (2010).
21. Aglipay, J. A., Martin, S. A., Tawara, H., Lee, S. W. & Ouchi, T. ATM activation by ionizing radiation requires *BRCA1*-associated *BAAT1*. *J. Biol. Chem.* **281**, 9710–9718 (2006).
22. So, E. Y. & Ouchi, T. The potential role of *BRCA1*-associated ATM activator-1 (*BRAT1*) in regulation of mTOR. *J. Cancer Biol. Res.* **1**, 3 (2013).
23. Zhang, C. J. et al. The Arabidopsis acetylated histone-binding protein *BRAT1* forms a complex with *BRP1* and prevents transcriptional silencing. *Nat. Commun.* **7**, 11715 (2016).
24. Choi, J. Y. et al. *CIDE* domains form functionally important higher-order assemblies for DNA fragmentation. *Proc. Natl Acad. Sci. USA* **114**, 7361–7366 (2017).
25. Lugovskoy, A. A., Zhou, P., Chou, J. J., McCarty, J. S. & Wagner, G. Solution structure of the *CIDE-N* domain of *CIDE-B* and a model for *CIDE-N/CIDE-N* interactions in the DNA fragmentation pathway of apoptosis. *Cell* **99**, 747–755 (1999).